CFD-3D and 1D modeling of fuel cell powertrain for a hydrogen vehicle

CFD-3D and 1D modeling of fuel cell powertrain for a hydrogen vehicle

Carmine Marra, Giuseppe Corda, Alessandro d'Adamo

Department of Engineering "Enzo Ferrari", University of Modena and Reggio Emilia, Via Vivarelli 10, Modena 41125, Italy

Contacts: carmine.marra@unimore.it, alessandro.dadamo@unimore.it

Abstract. As it is known the transport sector represents a major contributor to climate change. In particular, private transport contributes to the degradation of the air quality inside the cities or the residential areas. To address this issue, a progressive reduction of the use of fossil fuels as a primary energy source for these vehicles and the promotion of cleaner powertrain alternatives is in order. This study focuses on designing a fuel cell powertrain for a hydrogen-powered passenger car using numerical modeling. To this purpose, we initially modeled a base fuel cell and optimized its performance by using various materials for the bipolar plates and adjusting the platinum loading between the anode and cathode. Then, a preliminary design of the new powertrain has been proposed in order to achieve a nominal power of 100 kW and it has been tested on a WLTP 3b homologation cycle. Finally, we have been able to numerically estimate the behavior of the three main feeding line: hydrogen line, air line and cooling line. In conclusion, the obtained results demonstrate how numerical modelling can be successfully used in the design of complex systems such as those related to alternative energy. This work also provides a solid basis for the future development of increasingly efficient and environmentally friendly hydrogen vehicles.

1. Introduction

Over the past few years, public concern about air quality has increased. In particular, it is worth noting that about one-fifth of global CO_2 emissions come from internal combustion engines burning fossil fuels. In addition, air pollution from particulate matter, NO_x, SO_2 and CO, causes 9 million premature deaths per year worldwide. The above, coupled with increasingly stringent emissions regulations, have given increasing impetus to the automotive industry's commitment to the production of ultra-low emission vehicles (*or ULEV*). ULEVs currently on the market that are accessible to the general public include: hybrid electric vehicles (HEVs), plug-in hybrid electric vehicles (PHEVs), and extended-range electric vehicles (E-REVs). This changing landscape presents important opportunities for both economic growth and environmental protection.

For the purpose of reducing emissions, battery-powered vehicles are sufficient, provided that a sufficient electrical energy and power produced from renwable sources is available; however, this technology has several disadvantages compared to conventional internal combustion engine vehicle. In particular, short range, long charging times, and limited space for passengers and cargo due to the fact that batteries occupy a large volume on the vehicle have proven to be the main limitations of battery electric vehicles.

A complementary solution to battery electric vehicles are fuel cell vehicles, which fulfill the shortcomings of battery vehicles. In fact, assuming a hydrogen distribution network likewise that of common fuels, the experience of using an FCEV is comparable to that of a common internal combustion engine vehicle, still guaranting the absence of local pollutant emissions.

This paper presents a numerical study aimed at improving the performance of a fuel cell and a powertrain equipped with such power source. Firstly, the polarization curve was obtained and subsequently, improvements were made to enhance power output. The following paragraphs detail the modifications made and the results achieved. Furthermore, a 1D model of a vehicle with a fuel cell powertrain was used to test the cell's performance, characterized by three-dimensional simulation, on a WLTP Class 3b, in order to evaluate its behavior in real-world conditions.

2. Numerical Model

As mentioned, during this work, the fuel cell has been characterized by three-dimensional simulation, and then the whole vehicle with a fuel cell powertrain has been simulated. The numerical models adopted are presented below.

2.1. 1D Modelling

The starting vehicle model used is the one proposed by GT-SUITE to which some modifications has been made.

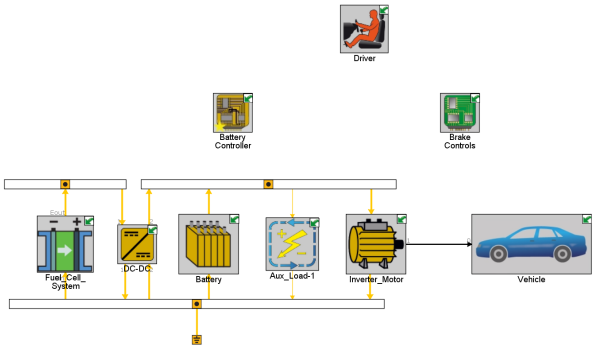

Figure 1: Vehicle Model FCHEV

In particular, changes were made in the fuel cell subsystem shown in figure 2. Continuing, in the DC-DC converter subsystem, the power management strategy was changed in order to obtain a SOC, at the end of the WLTP cycle, similar to the starting SOC.

In respect to this some details about this strategy are reported hereafter:

- When the battery SOC (State Of Charge) is higher than 90% the fuel cell is idling at 1 kW.
- Instead, when battery SOC is lower than 90% the fuel cell load is determined by the sum of vehicle load request and additional 5 kW in order to charge the battery.

It is important to note that the power management strategy for idling conditions and the associated auxiliaries consumption will be included in future works.

Instead, the battery subsystem was improved by removing some elements that made the modeling less realistic.

Finally, the power consumption by auxiliaries was added: the compressor, the hydrogen recirculation pump, the coolant recirculation pump, and the radiator fan.

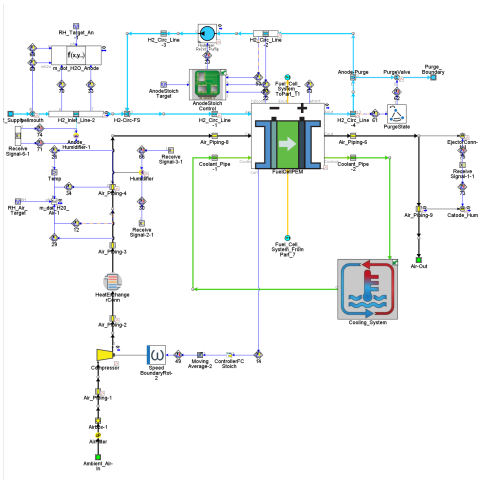

Figure 2: Balance of Plant of the FC subsystem

In particular, in this work GT-SUITE has been used which implements a logic whereby, during the reaction, hydrogen is removed from the anode, oxygen is removed from the cathode, and water vapor is added to the cathode. The rate at which this process occurs is calculated through the amount of electrons produced by the reaction, which, in turn, is determined through the current produced by the cell. While the heat generated by the cell depends on the electrochemical reaction and internal losses.

It is important to note that, as input, a polarization curve from 3D-CFD simulations results has been used, effectively coupling the 1D-3D simulation frameworks, but the actual performance of the cell is calculated dynamically based on specific operating conditions.

In particular the polarization curve provided by 3D-CFD results is assimilated to a reduced order model (0D model) as in equation 1:

$$V_{cell} = V_{OC} - V_{act} - V_{ohm} - V_{mt} \tag{1}$$

Where the open circuit potential is calculated as in equation 2:

$$V_{OC} = \frac{-\Delta \overline{g}_f}{2F} = \frac{-[(\overline{g}_f)_{H_2O} - (\overline{g}_f)_{H_2} - 0.5 \cdot (\overline{g}_f)_{O_2}]}{2F} \tag{2}$$

The activation losses are calculated as in equation 3:

$$V_{act} = \begin{cases} \frac{R_{gas} \cdot T}{2\alpha F}\left(\frac{i}{i_0}\right) & i \leq i_0/(1-\alpha) \\ \frac{R_{gas} \cdot T}{2\alpha F} \cdot \ln\left(\frac{i}{i_0}\right) & i > i_0/(1-\alpha) \end{cases} \tag{3}$$

Then the ohmic losses are calculated as in equation 4:

$$V_{ohm} = IR_{ohm} = iA_{cell}\left(\frac{t_m}{\sigma A_{cell}}\right) = \frac{i \cdot t_m}{\sigma_m} \tag{4}$$

where σ_m is the membrane ionic conducivity modelled as in equation 5:

$$\sigma_m = (b_{11}\lambda_m - b_{12}) \exp\left(b_2\left(\frac{1}{303} - \frac{1}{T_{cell}}\right)\right) \tag{5}$$

and λ_m is the membrane water content [12] as in equation 6:

$$\lambda_m = \begin{cases} 0.043 + 17.81a_m - 39.85a_m^2 + 36a_m^3 & 0 < a_m \leq 1 \\ min(16.14 + 1.4(a_m - 1)) & 1 \leq a_m \leq 3 \end{cases} \quad (6)$$

Finally the losses due to the mass transport are calculated as in equation 7:

$$V_{mt} = -C \cdot \ln\left(1 - \frac{i}{i_l}\right) \quad (7)$$

2.2. 3D Modelling

The three dimensional modeling is carried out with the commercial software Simcenter STAR-CCM+ licensed by Siemenes DISW. In particular, the governing equations for three-dimensional modeling of PEMFCs used in this work express the general conservation principles common to any CFD simulation, i.e., conservation of mass, momentum, energy, species, and charge.

However, it is important to decline these equations to the specific application of fuel cells. This can be done by noting that [5]:

- The flows are laminar, hence no turbulence models are needed
- Temporally, it is possible to consider stationary conditions since the typical time scales at which fuel cells operate are in the order of tens of seconds, if not minutes. This means that the simulations will be stationary, i.e. time-independent.
- The system is composed by different materials and therefore different physics, so dedicated modifications must be made to each equation.
- Flows within the cell may be multiphase, in particular the mixture multiphase (MMP) approach has been adopted to consider the presence of both liquid and gas phase water at cathode.
- In porous materials modeling, the macro-homogeneous approach has been used in order to describe material properties through average quantities.

Table 1: Steady-state governing equations applying the MMP model

	Equation
Continuity	$\nabla \cdot (\rho_{mix}\varepsilon\vec{V}_{mix}) = S_m$
Momentum	$\nabla \cdot (\rho_{mix}\varepsilon^2\vec{V}_{mix}\vec{V}_{mix}) = -\nabla p + \nabla(\mu\varepsilon\nabla \cdot \vec{V}_{mix}) + \vec{S}_V + \vec{S}_{cap}$
Species	$\nabla \cdot (\rho_{mix}Y_k\varepsilon\vec{V}_{mix}) = \nabla \cdot (\rho D_k^{eff}\nabla Y_k) + \vec{S}_k$
Energy	$\nabla \cdot [(\rho_{mix}c_p)^{eff}T\vec{V}_{mix}] = \nabla \cdot (k^{eff}\nabla T) + S_k$
Ionic Charge	$0 = \nabla \cdot (\sigma_e^{eff}\nabla\Phi_e) + S_{\Phi_e}$
Electrical Charge	$0 = \nabla \cdot (\sigma_s^{eff}\nabla\Phi_s) + S_{\Phi_s}$

The simulated cell is presented in detail below. In particular, a typical large-scale cell for the automotive sector with an active area of 300 cm^2 has been used. It is discretized with a structured mesh in order to obtain a conformal standard mesh with a total of 1508860 cells.

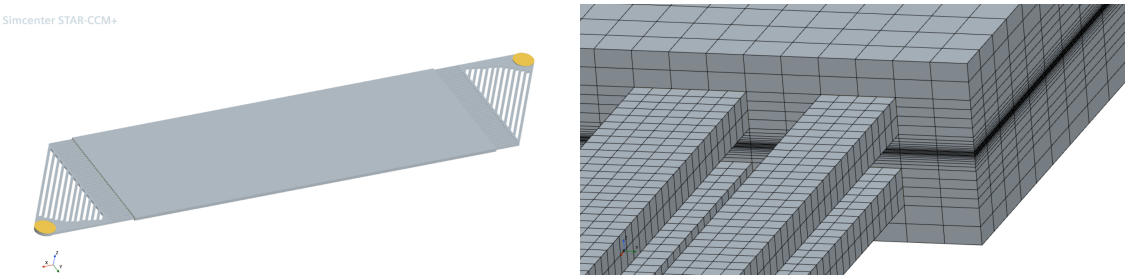

(a) Geometry (b) Detailed view of the mesh

Figure 3

3. Results

The first aim of the study was to obtain the polarization curve of the single cell through three-dimensional simulation. Due to time constraints, only two representative voltages on the polarization curve were identified. Following this, a complete curve was constructed by interpolating using a zero-dimensional model. Subsequently, the number of cells required to construct a fuel cell stack with a power rating of 100 kW was calculated. Then the cell so characterized with 3D simulation was implemented in the one-dimensional fuel cell vehicle model. The fuel cell stack was then tested by simulating a WLTP Class 3b driving cycle on a light-duty passenger car with dimensions and weights closely resembling the state-of-the-art FCEV, exemplified by Toyota Mirai.

Before proceeding to the analysis of the results, it is important to point out that the simulations were conducted not only with different materials, but also with different loadings of platinum. Therefore, the words "material 0.x - 0.y" on the graphs indicate that they refer to that particular material with an anode platinum loading of 0.x mg/cm^2 and a platinum loading at the cathode equal to 0.y mg/cm^2.

Some details about the vehicle are now reported. In particular, equals characteristics for battery and hydrogen tanks has been considered. So, the wheight of our vehicle has been estimated considering the Toyota Mirai weight of 1900 kg and then the weight of the fuel cell stack equipped by the Mirai (50 kg) has been subtracted from the total and the estimated weight of our stack has been added. This leads to a total weight of the vehicle equipped with the graphite BPs 0.4-0.4 equal to 1906 kg and a total weight of the vehicle equipped with the titanium BPs 0.2-0.6 equal to 1933 kg.

For what concerns the dimensions, equal dimensions to Mirai have been used on GT-SUITE for the characterizion of the vehicle.

After a preliminary screening of a broad selection of material for the bipolar plates we have decided to use titanium. The choiche was made due to the fact that the contact resistances of the titanium bipolar plates that we found in literature were the best and, in particular, it has been found by several groups that what matters most in order to maximize the output current from the cell is the condition of the membrane. For this reason, the use of materials with very low contact resistances allows the membrane to operate under increasingly better conditions regarding to its water content, ionic conductivity and temperature.

In particular, it is known that metals suffer in typical fuel cell working conditions so it is important to coat the plates in order to protect the metal from corrosion.

Since coated metal bipolar plates are not yet a standard in the industry, the only data that can be relied on are those found in the literature. However, it should be pointed out that the available data are referring to specific individual experiments, and since there is no single method of pretreating the plates before the coating is applied, nor there is a single method of applying

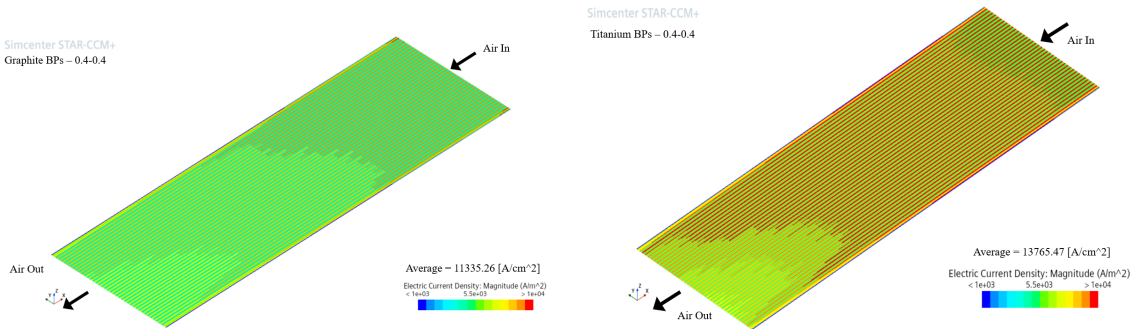

(a) Membrane ECD with graphite BPs 0.4-0.4 (b) Membrane ECD with titanium BPs 0.4-0.4

Figure 4

the coating itself, the data in literature regarding contact resistances may vary significantly. In addition, it should be considered that contact resistances vary significantly with the clamping pressure. That being said the values of conctacts resistance are from [10].

In particular, with the change of material an increase in current density produced by the membrane can be observed, as well as an increase of the homogeneity of its distribution on the membrane as can be seen in figures 4a and 4b.

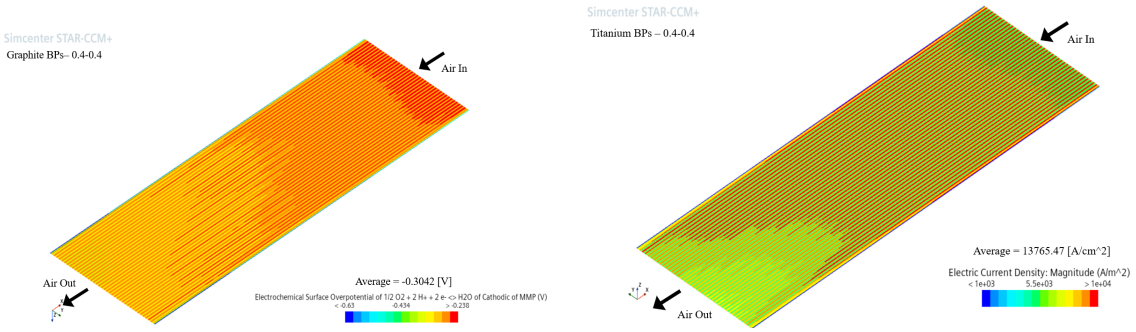

(a) Electrochemical Overpotential on cathode CL with graphite BPs 0.4-0.4 (b) Electrochemical Overpotential on cathode CL with titanium BPs 0.2-0.6

Figure 5

Then with the platinum imbalance between anode and cathode it has been possible to decrease the cathode-side activating overpotentials, as it can be seen in figures 5a and 5b. Note the negative values in the color scale for which higher values mean lower overpotential. In fact, as it is known, the cathode semireaction is the major rate-limiting process.

The superior performance visible through 3D is then confirmed when we take a look at the polarization and power curves of the two individual cells characterized as above and visible in figure 6.

3.1. Comparison Graphite 0.4-0.4 with Titanium 0.2-0.6

For the sake of brevity here it is reported only the comparison between the worst and the best cases. In figure 7, it can be seen the comparison between the polarization curves of the two candidate stacks consisting of 650 and 500 cells, where it can be seen that both stacks have a maximum power rating of 100 kW. In particular, it is important to note that all the data

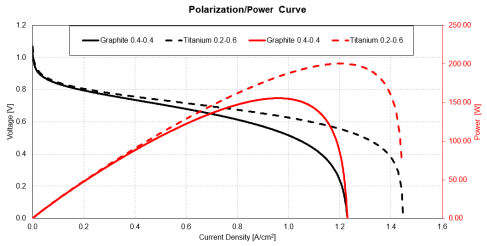

Figure 6: Polarization/Power curve comparison

represented in the various figures and tables below are based on the values given in the table 5 in appendix.

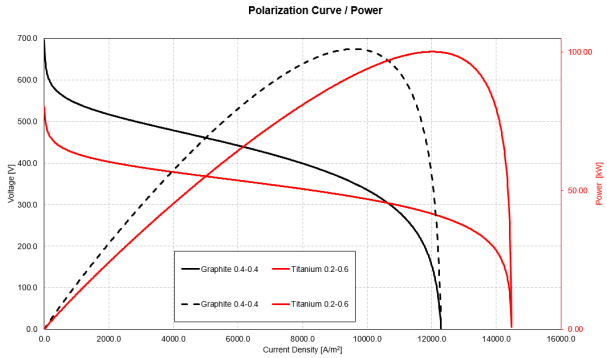

Figure 7: Stack polarization/power curve comparison

Before moving on to the direct comparison, however, it is necessary to specify that for graphite a cost of 12.5 €/kg has been estimated, while for grade 1 titanium, used in this work, although the data are highly variable and generally difficult to find, the estimate made is 10 €/kg. Regarding the cost of titanium, it should be noted that the price of the coating was not considered, which could greatly increase the estimated value (e.g. in case of gold coating).

After providing this necessary introduction, a comparison between the two stacks can be made. Firstly, as Figure 8a highlights, in order to achieve the same power rating, the graphite bipolar plate cell requires a larger number of cells compared to the titanium cell, resulting in an estimated increase of 20% in the number of cells required. This leads to higher overall costs and occupied volume. It is noteworthy that the only disadvantage of the titanium bipolar plate stack is its higher global weight, due to the higher density, despite requiring fewer cells. This result is based on the comparison being made at the same bipolar plate volume. However, it should be noted that a titanium bipolar plate offers greater structural stiffness than graphite, even with a smaller overall volume. Therefore, a suitable evaluation can result in the development of a less bulky, hence less heavy and less expensive bipolar plate that can be used to create the stack.

In particular, analyzing the figure 8b shows that the overall cost savings are not so much due to the bipolar plates, but rather to all the other components in the cell. In fact, since the number of cells in the stack with titanium bipolar plates is lower, there is also a lower cost on the total of each component. The cost of BPs is higher in our study conducted at equal volume due to the methodology we employed, which calculates the price of each component by multiplying the density, volume, and price over weight. Consequently, the price of titanium BPs is particularly elevated due to its significantly high density. Note that the properties of the materials used in this study are available in table 6 in appendix.

Furthermore, from figure 9, it can be seen that the stack with titanium bipolar plates has some big advantages: a decrease in the price-over-power and price-over-weight ratio of 17% and 41%, respectively, and an increase in the power-over-volume ratio of 22%. In contrast, the only disadvantage is a 28% decrease in the power-over-weight ratio due to the higher weight of the stack.

Once the stacks have been compared in absolute value, it is then necessary to observe their behavior on the driving cycle. First, we have to point out that the power flow management strategy adopted is designed to use intensively the fuel cell and, therefore, to complete the driving cycle with the battery at the same initial SOC. In particular, it was observed that in general, the power output behavior has only minor differences due to the fact that the titanium stack vehicle is slightly heavier. In addition, other trends such as stack temperature trends and heat generated remain almost similar, depending essentialy on voltage and nominal power. Therefore, it is possible to present the results and to compare the average data of the three main lines.

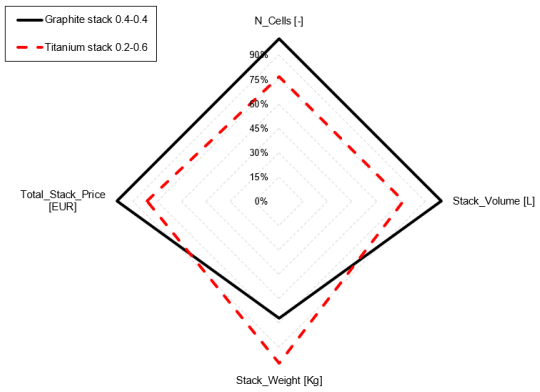

(a) Overall dimensions, weights, and costs

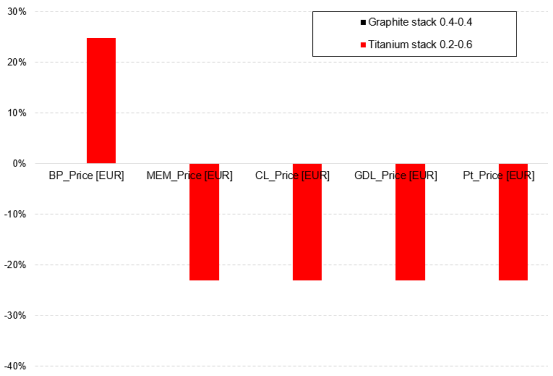

(b) Relative variation of cost of individual components with respect to graphite (baseline, assumed 0% reference). See value in Appendix for the absolute values

Figure 8

First, the comparison on the hydrogen line can be seen in table 2. In particular, there is a slightly higher consumption of hydrogen, these results are due to the fact that the stack equipping the vehicle with titanium bipolar plates is heavier and, as a result, must deliver a higher amount of power. But this is not substantial and does not lead to significant disadvantages of one solution over the other.

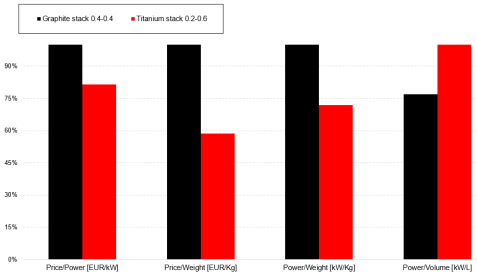

Figure 9: Trend of ratios of weight, cost, power, and volume

	Graphite stack	**Titanium stack**
Mass of hydrogen consumed [kg]	0.295	0.302
Hydrogen consumption [kg/100 km]	1.274	1.302
Amount of hydrogen required for 500 km [kg]	6.37	6.51
Distance traveled with 5.5 kg of H_2 [km]	431.73	422.48

Table 2: Hydrogen line Graphite 0.4-0.4 and Titanium 0.2-0.6

As for the air line, shown in the table 3, the compressor consumes more power on average and has a higher peak power. It should be noted, however, that it works on average at higher efficiencies partly compensating for the higher power demand.

	Graphite stack	**Titanium stack**
Average compressor power input [kW]	1.51	1.70
Average working efficiency of the compressor [-]	74.40	74.65
Maximum power absorbed by the compressor [kW]	17.06	20.08
Total water produced [kg]	2.30	2.38

Table 3: Air line Graphite 0.4-0.4 and Titanium 0.2-0.6

In conclusion, the coolant line data are shown in the table 4, where a large increase in the amount of coolant fluid passing through the radiator can be seen, probably due to the fact that as the vehicle weights more, the cell has to generate more power and consequently the cooling circuit has to dissipate more heat.

	Graphite stack	**Titanium stack**
Average flow rate in the cooling circuit [L/h]	4691.99	4862.41
Average flow rate through the radiator [L/h]	416.81	661.15
Average power of the recirculation pump [kW]	0.064	0.1

Table 4: Coolant line Graphite 0.4-0.4 and Titanium 0.2-0.6

Despite this, the average pump consumption increases by a negligible amount, while the peak power of the refrigerant recirculation pump increases from 0.55 kW to 0.9 kW.

4. Conclusions

The work aimed to develop a preliminary methodology capable of simulating a vehicle equipped with a fuel cell powertrain through the combined use of CFD-3D and 1D modeling. Three-dimensional modeling is part of the know-how of the research group in which this work is included, and its reliability is used to accurately predict fuel cell performance. Indeed, thanks to three-dimensional modeling, it has been possible to evaluate the increase in performance of

a fuel cell that occurred due to to the improvement of the materials used for the bipolar plates and the better use of platinum loading between anode and cathode. In particular, simulations have shown that the variation of bipolar plate materials and the unbalance of platinum loading can have a significant impact on the performance of the fuel cell.

That said, the one-dimensional modeling of the entire FCEV was the added value brought by the present work. Specifically, through the one-dimensional simulation, it was possible to compare the various fuel cells and how their performance are reflected on the whole vehicle. In particular, it is striking the comparison between a stack with graphite bipolar plates and a 0.4-0.4 loading of platinum and a stack with titanium bipolar plates and platinum loading of 0.2-0.6. In fact, the results suggest the importance of having a cell with a polarization curve that is as horizontal as possible in order to get a stack as contained as possible. From this point of view, the savings are relevant on several points: economic, weight and volume. In addition, the choice of power flow management strategy is of paramount importance, as it as it greatly afflicts hydrogen consumption, as well as the heat to be dissipated and thus all the power consumption by auxiliaries.

The presented methodology will be further developed in future works to account for more advanced energy managment strategies and to implement innovative solutions at a cell level.

5. Appendix

	Graphite stack 0.4-0.4	**Titanium stack 0.2-0.6**
N_Cells [-]	650.00	500
Power [kW]	100.00	100.00
BP_Weight [Kg]	50.87	76.14
MEM_Weight [Kg]	1.17	0.90
CL_Weight [Kg]	0.59	0.45
GDL_Weight [Kg]	6.83	5.25
Pt_Weight [Kg]	0.16	0.12
BP_Price [EUR]	610.39	761.40
MEM_Price [EUR]	190.24	146.34
CL_Price [EUR]	16.22	12.47
GDL_Price [EUR]	189.19	145.53
Pt_Price [EUR]	5299.94	4076.88
Stack_Volume [L]	18.53	14.26
Stack_Weight [Kg]	59.60	82.86
Total_Stack_Price [EUR]	6305.98	5142.62
Price/Power [EUR/kW]	62.44	51.43
Price/Weight [EUR/Kg]	105.80	62.06
Power/Weight [kW/Kg]	1.69	1.21
Power/Volume [kW/L]	5.45	7.01

Table 5: Comparison of Graphite Stack 0.4-0.4 with Titanium 0.2-0.6

Properties	Titanium	Graphite
Thermal Conductivity IP $[W/(mK)]$	16.5	95
Thermal Conductivity TP $[W/(mK)]$	8.25	47.5
Electrical Conductivity IP $[S/m]$	$4.93E+05$	$5.12E+05$
Electrical Conductivity TP $[S/m]$	$2.47E+05$	$2.56E+05$
Density $[kg/m^3]$	3600	1850
Specific Heat $[J/(kgK)]$	630	707.68
Thermal contact resistance $[m^2K/W]$	$2.96E-04$	$3.00E-04$
Electrical contact resistance $[m^2 \cdot \Omega]$	$2.00E-07$	$8.00E-07$

Table 6: Properties of tested materials

6. References

[1] Barbir, F. PEM Fuel Cells: Theory and Practice. (Elsevier,2005)
[2] Corda, G., Cucurachi, A., Diana, M., Fontanesi, S. & D'Adamo, A. A Methodology to Design the Flow Field of PEM Fuel Cells. (SAE Technical Paper,2023), https://doi.org/10.4271/2023-01-0495
[3] Corda, G., Fontanesi, S. & D'Adamo, A. Numerical Comparison of the Performance of Four Cooling Circuit Designs for Proton Exchange Membrane Fuel Cells (PEMFCs). *SAE Technical Papers*. (2022), https://doi.org/10.4271/2022-01-0685
[4] D'Adamo, A. & Borghi, M. On the use of tapered channels gas distributors to promote convection in PEM Fuel Cells. *E3S Web Of Conferences*. **312** pp. e07018 (2021,9), DOI: 10.1051/e3sconf/202131207018
[5] D'Adamo, A., Haslinger, M., Corda, G., Höflinger, J., Fontanesi, S. & Lauer, T. Modelling Methods and Validation Techniques for CFD Simulations of PEM Fuel Cells. *Processes*.**9** (2021), https://doi.org/10.3390/pr9040688
[6] D'Adamo, A. & Corda, G. Numerical Simulation of Advanced Bipolar Plates Materials for Hydrogen-Fueled PEM Fuel Cell. (SAE Technical Paper,2022), https://doi.org/10.4271/2022-01-0683.
[7] D'Adamo, A., Riccardi, M., Borghi, M. & Fontanesi, S. CFD Modelling of a Hydrogen/Air PEM Fuel Cell with a Serpentine Gas Distributor. *Processes*. **9** (2021), https://doi.org/10.3390/pr9030564
[8] D'Adamo, A., Riccardi, M., Locci, C., Romagnoli, M. & Fontanesi, S. Numerical Simulation of a High Current Density PEM Fuel Cell. (SAE Technical Paper,2020), https://doi.org/10.4271/2020-24-0016
[9] Goshtasbi, A., Pence, B. & Ersal, T. Computationally Efficient Pseudo-2D Non-Isothermal Modeling of Polymer Electrolyte Membrane Fuel Cells with Two-Phase Phenomena. *Journal Of The Electrochemical Society*. **163** pp. F1412-F1432 (2016,10)
[10] Gou, Y., Chen, H., Li, R., Geng, J. & Shao, Z. Nb–Cr–C coated titanium as bipolar plates for proton exchange membrane fuel cells. *Journal Of Power Sources*. **520** pp. 230797 (2022)
[11] Hermann, A., Chaudhuri, T. & Spagnol, P. Bipolar plates for PEM fuel cells: A review. *International Journal Of Hydrogen Energy*. **30**, 1297-1302 (2005), Cancun 2003
[12] Springer, T., Zawodzinski, T. & Gottesfeld, S. Polymer Electrolyte Fuel Cell Model. *Journal Of The Electrochemical Society*. **138**, 2334 (1991,8), https://dx.doi.org/10.1149/1.2085971
[13] Larminie, J. & Dicks, A. Fuel Cell Systems Explained. (John Wiley,2003)
[14] Lohse-Busch, H., Stutenberg, K., Duoba, M. & Iliev, S. Technology Assessment Of A Fuel Cell Vehicle: 2017 Toyota Mirai. (2018,1)
[15] O'Hayre, R. Fuel cell fundamentals. (John Wiley,2016)
[16] Xie, B., Zhang, G., Xuan, J. & Jiao, K. Three-dimensional multi-phase model of PEM fuel cell coupled with improved agglomerate sub-model of catalyst layer. *Energy Conversion And Management*. **199** pp. 112051 (2019)
[17] Zawodzinski, T., Springer, T., Davey, J., Jestel, R., Lopez, C., Valerio, J. & Gottesfeld, S. A Comparative Study of Water Uptake By and Transport Through Ionomeric Fuel Cell Membranes. *Journal Of The Electrochemical Society*. **140**, 1981 (1993,7)
[18] Zawodzinski, T., Neeman, M., Sillerud, L. & Gottesfeld, S. Determination of water diffusion coefficients in perfluorosulfonate ionomeric membranes. *The Journal Of Physical Chemistry*. **95**, 6040-6044 (1991)